



**HAL**  
open science

# Experimental and Numerical Evaluation of Toxic Pool Evaporation

Benjamin Truchot, André Carrau, Véronique Debuy, Thibault Penelon,  
Jean-Pierre Bertrand

► **To cite this version:**

Benjamin Truchot, André Carrau, Véronique Debuy, Thibault Penelon, Jean-Pierre Bertrand. Experimental and Numerical Evaluation of Toxic Pool Evaporation. Applied Sciences, 2020, 10 (23), pp.8448. 10.3390/app10238448. ineris-03318336

**HAL Id: ineris-03318336**

**<https://ineris.hal.science/ineris-03318336>**

Submitted on 9 Aug 2021

**HAL** is a multi-disciplinary open access archive for the deposit and dissemination of scientific research documents, whether they are published or not. The documents may come from teaching and research institutions in France or abroad, or from public or private research centers.

L'archive ouverte pluridisciplinaire **HAL**, est destinée au dépôt et à la diffusion de documents scientifiques de niveau recherche, publiés ou non, émanant des établissements d'enseignement et de recherche français ou étrangers, des laboratoires publics ou privés.

Article

# Experimental and Numerical Evaluation of Toxic Pool Evaporation

Benjamin TRUCHOT <sup>1,\*</sup>, André CARRAU <sup>2</sup>, Véronique DEBUY <sup>1</sup>, Thibault PENELON <sup>1</sup> and Jean-Pierre BERTRAND <sup>1</sup>

<sup>1</sup> INERIS, Parc Technologique ALATA, 60550 Verneuil en Halatte, France; veronique.debuy@ineris.fr (V.D.); thibault.penelon@ineris.fr (T.P.); jean-pierre.bertrand@ineris.fr (J.-P.B.)

<sup>2</sup> EDF, DIPDE, 8 cours André Philip, 69100 Villeurbanne, France; andre.carrau@edf.fr

\* Correspondence: benjamin.truchot@ineris.fr; Tel.: +33-(0)3.44.61.81.50

Received: 30 September 2020; Accepted: 25 November 2020; Published: 26 November 2020

**Abstract:** To date, safety distances to toxic pool evaporation as measured by known models have been quoted in hundreds of meters, without a deeper study of the time variation of the evaporation rate. In order to evaluate this specific aspect, we designed an experimental study. This study included small-scale tests with a 0.1 m<sup>2</sup> evaporating pool, and medium-scale tests with 1 and 2 m<sup>2</sup> evaporating pools. For both small- and medium-scale tests, the experimental vertical velocity profile was built to reproduce an atmospheric profile after applying the Froude scaling procedure. The scope of this study focused on ammonia pool evaporation, with each test lasting long enough to highlight the time evolution of the evaporation rate. While many other parameters may have strongly influenced the evaporation rate, the influence of the most classical parameters was tested, including pool concentration, wind velocity, and ambient turbulence. During these tests, the metrology was designed to enable the measuring of evaporation rates with great precision, but other important components were also measured. This series of tests clearly showed a strong variation of the evaporation rate in the first 30 minutes after the release—the evaporation rate dropped to 20% of its initial value after this 30-min period. It is therefore obvious that such reactions should strongly influence the toxic consequences of the vapor atmospheric dispersion. The known influence of other parameters was also confirmed—typically, the higher the pool concentration and/or wind velocity, the higher the evaporation rate. The surrounding turbulence effect was also taken into consideration and was proven to have a lower influence on the evaporation rate. In light of these experiments, we present below a physical model named EVAP-Tox used to estimate the time variation of the evaporation rate of an ammonia solution.

**Keywords:** pool evaporation; ammonia solution; medium-scale test

---

## 1. Introduction

In the context of land use planning, toxic dispersion modelling resulting from pool evaporation determines the safety distance to be in the hundreds of meters to avoid possible negative human consequences. These distances are based on computations of both the source term evaluation and the dispersion modelling hypothesis. For the purpose of this particular study, the source term is of primary importance. The objective of this paper was to evaluate the time evolution of ammonia solution evaporation rate. This product was selected because it is largely used in the industry in various concentrations, typically for water treatment in nuclear power stations. In most existing models, as described in the next section, the evaporation rate is assumed to be constant.

### 1.1. Brief Overview

Before describing the experimental set-up and corresponding results, it is important to give some background about the expected phenomena, since these physical phenomena govern the experimental design.

Evaporation models are commonly based on the boundary layer theory of Sutton [1], which considers the advection–diffusion equation [2]. This approach, combined with experiments, has allowed several evaporation models to be developed, each on the basis of a specific situation [3–9]. Several comparisons between those correlations have been published in the literature, for example, in [10].

The Mackay and Matsugu correlation formula, although now quite old, is still widely used in the context of risk management and land use planning, and therefore it was used as a basis for our experimentation. While simplified in some cases [11], the Mackay and Matsugu correlation was originally written as follows:

$$q_{ev} = k_m (P_v - P_\infty) M / RT_p \quad (1)$$

$q_{ev}$  evaporation rate (kg/s);

$P_v$  vapor pressure at the pool temperature and concentration (Pa);

$P_\infty$  vapor pressure at the boundary layer limit (Pa);

$M$  molar weight (kg/mol);

$R$  Universal gas constant (8.31 J/mol.K);

$T_p$  pool temperature (K).

The mass transfer coefficient,  $k_m$ , is written as

$$k_m = C_{m\&m} U^{0.78} (2 * r_p)^{-0.11} Sc^{-0.67} \quad (2)$$

$C_{m\&m}$  Mackay and Matsugu coefficient ( $4.786 \cdot 10^{-3}$ );

$U$  air velocity 10 m above the pool surface (m/s);

$r_p$  pool radius (m)– $2 * r_p$  represents the pool diameter or, for non-circular pools, to the wind-exposed pool length;

$Sc$  Schmidt number.

One of the key criteria in Equation (1) is the product's vapor pressure. This quantity is a function of both the pool's temperature and concentration (Figure 1) but is considered as a constant in the equation.

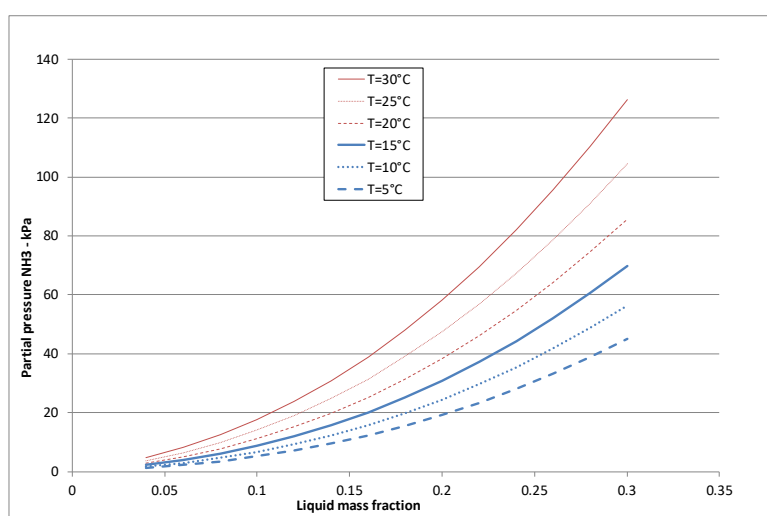


**Figure 1.** Evolution of the vapor pressure for ammonia as a function of temperature and pool concentration.

Regarding toxic pools, most evaporation models used in the industry literature are based on a constant vapor pressure during the evaporation process. Very few papers have dealt with the

unsteady process of evaporation [12]. On the basis of experiments with hydrogen chloride, the authors of [12] claim that a concentration gradient occurs over time and leads to an unsteady phenomenon. Such a concentration gradient may strongly influence the evaporation rate of ammonia, and thus it was specifically investigated in this paper. This evolution over time was also studied for hydrocarbons, taking temperature evolution into consideration [13–15]. Some authors specifically studied the evolution of evaporation rate of concentrated ammonia solutions in small-scale pools without wind [16] or with assessing the influence of wind [17,18].

This paper presents a new series of experimental tests for ammonia evaporation, taking into consideration various parameters such as pool concentration and its temperature and the ambient humidity. Two different scales were used to evaluate the influence of the scale factor by modifying the pool size.

### 1.2. Consequences Regarding Experimental Design

On the basis of the aforementioned physical phenomena, some parameters appeared to be of primary importance to the experimental design. The first is wind profile since the evaporation rate is based on the ambient wind velocity. The second parameter is the evaporation rate over a specific period of time to be measured at an adequate frequency. The last parameter is the pool temperature, since this parameter strongly influences vapor pressure and, consequently, the evaporation rate.

## 2. Experimental Set-Up

### 2.1. General Considerations

Evaporation tests were conducted in INERIS' fire test installations [19], more precisely in the 10 m<sup>3</sup> room for small-scale tests and in the fire gallery for medium-scale tests. Pictures of the installations are presented below in Figure 2. The sections were 0.465 m wide and 0.165 m high for the small-scale tests and approximately 3 m × 3 m for the medium-scale tests.



**Figure 2.** Picture of the pool photography and instrumentation for small (**left**) and medium (**right**) scales.

The scale factor for the tests is based on a Froude scaling. Considering the Froude number,  $Fr = U^2/(g.l)$ , where  $l$  stands for a characteristic length,  $g$  for gravity, and  $U$  for representative velocity, we were able to evaluate the different physical quantities on the basis of length scaling. The actual pool was based on a basic size of 100 m<sup>2</sup>, 10 m × 10 m. The corresponding scale factor on length,  $\sigma$ , can then be defined. For a given scale factor  $\sigma$  on length, the scale factor for the velocity is  $\sqrt{\sigma}$  to conserve the Froude number. For small-scale tests, the pool was 0.1 m<sup>2</sup>, 0.316 m × 0.316 m, and 0.03 m deep. In this case,  $\sigma$  was equal to 31.6. For medium-scale tests, the reference size was 1 m<sup>2</sup>, 1 m × 1 m, and  $\sigma$  was equal to 10; the pool depth was also 3 cm.

As previously mentioned, one of the key factors when studying pool evaporation is being able to reproduce a relevant velocity profile above the pool. Considering the atmospheric dispersion as

target application, the velocity profile in both the small- and medium-scale tests were designed to be as close as possible to an atmospheric profile, somewhere between neutral and stable conditions. The reference velocity profiles for medium-scale tests are shown in Figure 3. “Right” and “left” on this figure indicate that the measure was taken in the center of the section where the ammonia pool was, right and left near the limit of the pool, in the same section of the duct. The reference experimental velocity was measured 1 m above the pool since the scale factor was 10 for length, with a reference experimental value of 1 m/s corresponding to a “real” velocity of 3.2 m/s, since the scale factor for velocity is  $\sqrt{10}$  for a Froude scaling.

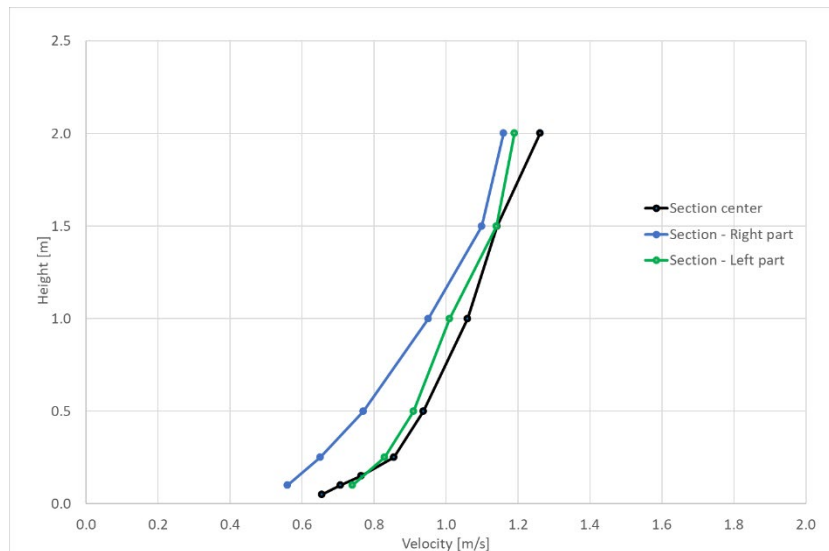


Figure 3. Velocity profile for medium-scale configuration.

To ensure a realistic turbulence intensity in this profile, we managed the flow before it reached the pool using obstacles distributed on the ground. Pictures of the installations, including obstacle distribution and pool, are reproduced in Figure 4 for both scales. Small-scale obstacles were 55 mm long, 21 mm wide, and 21 mm high; the inter-obstacle distance was 2 cm along the wind direction and 5 cm in the other direction. They were distributed over an area 700 mm upstream of the pool. For large-scale tests, obstacles were approximate cubes with a length of 600 mm and were distributed over 15 m upstream of the pool. Distance between obstacles was about 60 cm in both directions.



Figure 4. Picture of obstacle distribution for small (left) and medium (right) scales.

The turbulent velocity measured in the duct using a high-speed MacCaffrey probe [20,21] prior to the evaporation was about 4% of the averaged value for the 1 m/s tests.

An additional configuration was tested by generating artificial turbulence upstream of the pool. A specific system that included horizontal obstacles was then used for the medium-scale test, as shown in Figure 5. This system dimensions were 1 m width and 10 cm height.



**Figure 5.** Picture of the system used to generate artificial turbulence upstream of the pool.

## 2.2. Metrology

The most important quantity we wanted to measure for this particular study was the evaporation mass flow rate. It was actually measured using two complementary techniques. The first simply consisted of weighting the pool over time, while the second used a FTIR (Fourier transform infrared) spectrometer to evaluate atmospheric concentration downstream of the pool, coupled with a total mass flow rate in the ventilation section. The FTIR sampling probe was placed in the vertical part of the duct for the small-scale test and in the middle of a 5 m long restricted section for the medium-scale test. The measurement frequency of the FTIR was set at 1 Hz. Using velocity and temperature measurements, it directly led to the evaporation flow rate. Before each test, the mass concentration of the solution was measured. To prevent any interaction between the evaporated vapor and the different surrounding solids, we made the concentration measurement as close as possible to the pool using a dedicated mixing system to ensure a perfectly mixed air. The mixing system consisting of a reduced section to obtain a more homogeneous mixture was validated on the basis of the measurement of resulting very low concentration fluctuations. The mixture's homogeneity was then verified through the lack of fluctuation when measuring concentration with the FTIR. All solid surfaces between the pool and the FTIR sampling probe were covered by Teflon. Mean velocity and velocity fluctuations were measured using MacCaffrey probes [20] associated with a pressure transducer. The velocity was measured close to the pool, in the middle of the duct height, for each test. In addition, velocity profile was determined using several points at different heights. Following [21], the probes also enabled us to estimate the turbulent velocity, which was 4% of the average velocity. Data frequency was then set at 10Hz.

To confirm the accuracy of the FTIR and air flow rate methods used for evaluating the evaporation rate, we compared the results to measurements obtained by two other methods. The first was the weight measurement of the pool described above and the second consisted in pool concentration measurement before and after the tests. Concentration in the solution after the test was measured using pool sampling after a mixing process to ensure a homogenous concentration. Those two results confirmed the ones obtained using the FTIR and flow rate methods. Other specific sampling was taken to evaluate the concentration at different heights.

Pool temperature was also measured using several PFA (Perfluoroalkoxy)-covered K-type thermocouples placed in the pool's depth. While the response time is usually higher than with uncovered thermocouples, these specific ones were chosen because of their corrosion resistance. They were placed near the bottom of the pool, then 0.015 m and 0.0275 m above the bottom of the pool.

### 2.3. Experimental Design

As previously mentioned, the objective of this study was to determine a realistic evaporation rate for ammonia under various conditions. To meet this objective, we carried out 6 tests at the small scale and 5 at the medium scale. For both configurations, concentrations were precisely measured before running the tests, since this parameter is of primary importance for evaporation modelling. Table 1 below lists the smaller scale tests, with the comparison reference test highlighted in blue (test no. 3).

**Table 1.** Presentation of the small-scale tests. Concentration given by the provider is given in brackets ( ).

| Test No. | Mass Concentration of the Pool (%)* | Air Velocity (m/s) | Ambient Turbulence | Pool Surface (m <sup>2</sup> ) | Initial Pool Temperature (°C) | Ambient Air Temperature (°C) |
|----------|-------------------------------------|--------------------|--------------------|--------------------------------|-------------------------------|------------------------------|
| 1        | 17.0% (21%)                         | 1 m/s              | Low                | 0.1                            | 3 °C                          | 1.1 °C                       |
| 2        | 18.6% (21%)                         | 1 m/s              | Low                | 0.1                            | 4.7 °C                        | 6.5 °C                       |
| 3        | 29.4% (30%)                         | 1 m/s              | Low                | 0.1                            | 0.3 °C                        | 3.2 °C                       |
| 4        | 29.5% (29%)                         | 1.5 m/s            | Low                | 0.1                            | 2.2 °C                        | 3.3 °C                       |
| 5        | 29.0% (29%)                         | 0.5 m/s            | Low                | 0.1                            | 2.2 °C                        | 2.2 °C                       |
| 6        | 26.5% (24.6%)                       | 1 m/s              | Low                | 0.1                            | 1.4 °C                        | 4.5 °C                       |

On the basis of the small-scale test results, we designed a series of 5 tests at the medium scale in order to confirm the small-scale observations and, when required, to go further. The reference test for medium-scale tests is also highlighted below in blue (test no. 1). Tests marked with a star (tests no. 1, 2, and 5) in Table 2 correspond to those made with comparable conditions during small- and medium-scale tests (such tests are crucial to discuss the influence of the scale factor).

**Table 2.** Presentation of the medium scale tests. Concentration given by the provider is given in brackets ( ).

| Test No. | Mass Concentration of the Pool (%)* | Air Velocity (m/s) | Ambient Turbulence | Pool Surface (m <sup>2</sup> ) | Initial Pool Temperature (°C) | Ambient air Temperature (°C) |
|----------|-------------------------------------|--------------------|--------------------|--------------------------------|-------------------------------|------------------------------|
| 1 *      | 27.9% (29%)                         | 1.0                | Low                | 1                              | 15.2 °C                       | 14.9 °C                      |
| 2 *      | 28.2% (29%)                         | 1.5                | Low                | 1                              | 12.7 °C                       | 12.1 °C                      |
| 3        | 27.85% (29%)                        | 1.0                | Low                | 2                              | 13.0 °C                       | 13.8 °C                      |
| 4        | 28.36% (29%)                        | 1.0                | High               | 1                              | 14.9 °C                       | 14.4 °C                      |
| 5*       | 27.65% (29%)                        | 1.0                | Low                | 1                              | 12.7 °C                       | 12.5 °C                      |

Significant variations of the mass concentration and initial temperatures of the pool can be noticed. Since the installations are opened to the outdoors, temperature control was not possible. Therefore, a 10 °C difference can be seen between the two scales, which should be kept in mind when interpreting the results. As for the concentration, the difference was due to the fact that we chose to give the actual measured concentration rate instead of the manufacturer's 29% value; this also shows that when dealing with real situations for risk management, the actual concentration can differ from the estimated one. This actual concentration was measured in our chemistry laboratory (ion chromatography).

During the experiment, the pool was filled with the ammonia solution, and evaporation was considered to start after the pool was completely filled.

### 3. Small-Scale Test Results

#### 3.1. Experimental Results: Reference Case

While one objective of this study was to characterize the evaporation rate evolution over time, the initial evaporation rate was compared with the existing correlations, mainly the one proposed by [3] (Equations (1) and (2)), since it is widely used in safety evaluation. Consequently, on the different graphs showing the evaporation rate over time, we also plotted a horizontal line representing the evaporation rate estimated using the Mackay and Matsugu correlation [3], calculated using the initial conditions of the pool.

The first result obtained from this study was the confirmation of the tendency observed by [16,18], the large reduction of the evaporation rate over time. The evaporation rate over time for the reference case is plotted in Figure 6, together with the pool's temperature. The grey interval around the red curve represents the uncertainty interval. These uncertainties were evaluated considering the different uncertainties along the measurement chain. This implies considering the uncertainties in the concentration measurement and in the velocity measurement, including density, duct section, and pressure due to the measuring system.

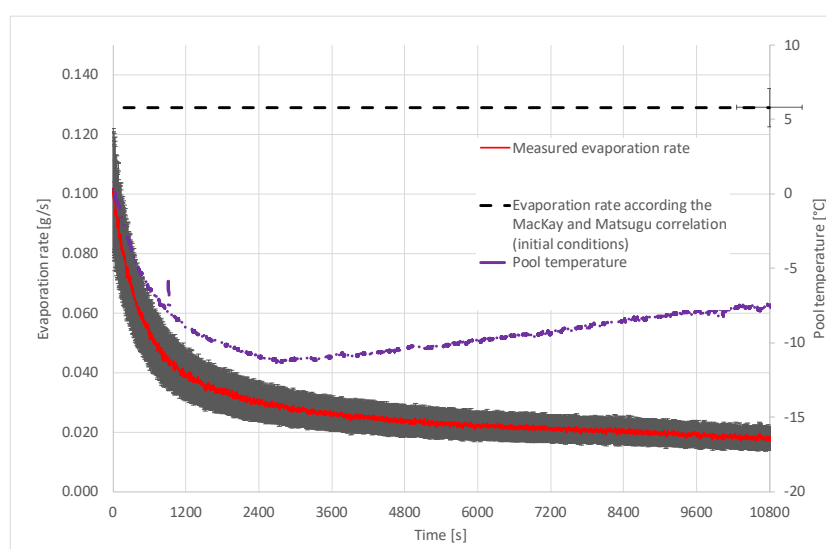


**Figure 6.** Evaporation rate and pool temperature over time for the small-scale reference case. The grey zone represents the uncertainties.

This curve clearly highlights the time evolution of the evaporation rate with a strong diminution during the first hour, when the evaporation rate is divided by almost 5 and then a more constant evaporation rate. Introducing such a difference in dispersion model, i.e., a division by 5 of the evaporation rate, means a strong reduction of the gas quantity emitted into the atmosphere and consequently a lower concentration in the atmosphere. An important consequence of this observation is a reduction of the safety distance where the toxic threshold is reached. Another observation in the figure above is that the evaporation rate estimated using the Mackay and Matsugu correlation was close to the initial measurements, keeping in mind that in this case, the correlation overestimated the evaporation rate.

#### 3.2. Influence of Pool Temperature

One of the main parameters that influences the evaporation rate is vapor pressure. This quantity depends on both the pool's concentration and temperature. Therefore, it is crucial to estimate their influence during the test. The temperature curve in Figure 6 above shows that temperature was reduced by about 12 °C after 40 min. Such a temperature variation would induce an evaporation rate reduction of about only 24%. This means that the temperature alone did not explain the measured evaporation rate reduction, which exceeded 80%. The increase in pool temperature observed after the

first hour or so can be explained by cooling reduction due to the evaporation process, while heating sources, conduction, and convection stayed quite constant. This specific behavior of the temperature concentration was also presented by [18]. It is important to note that during the tests, temperature was measured over three heights: near the surface, in the middle depth of the pool, and near the bottom. The pool temperature remained quite homogeneous along its depth during the evaporation process (see Figure 7). This curve shows that, after 1 hour, the temperature difference between the surface and the bottom of the pool was less than 1 °C. Such a small difference is not relevant for evaporation modelling and can therefore be neglected.

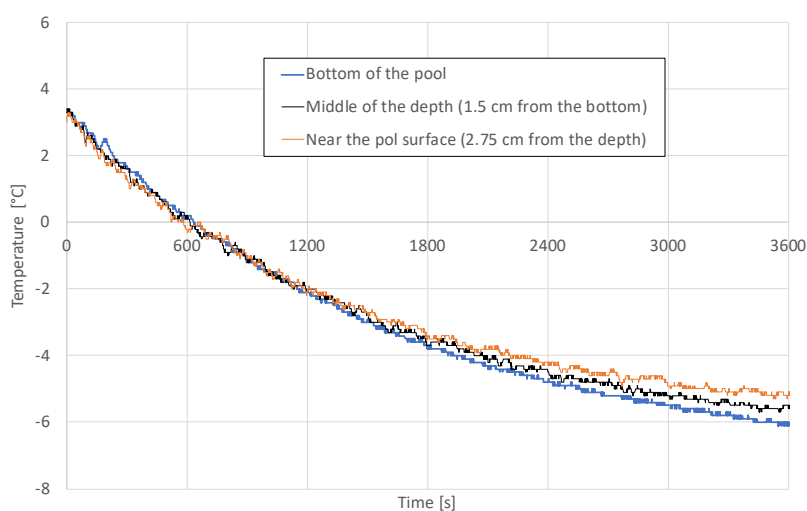


**Figure 7.** Temperature evolution at three depths for the small-scale reference case.

### 3.3. Influence of Concentration Gradient on the Vapor Pressure

As mentioned in Section 1.1, vapor pressure, a key factor for evaporation, is also a function of the pool's concentration. To estimate this influence, we performed a reverse computation. Integrating the measured evaporation rate gives the total quantity of ammonia lost by the pool. This enables one to compute the theoretical concentration, assuming a homogeneous concentration. For the present configuration, it should be 24%. For such a 24% ammonia concentration, the final evaporation rate, computed using this concentration and the measured temperature, should have been 55% of the initial value. This estimation does not consider that a given part of water also evaporates, leading to a higher homogeneous concentration and associated evaporation rate.

Considering that the final evaporation rate is about 20% of the initial value, this implies that the concentration at the pool surface would be lower than the homogenous estimated value, demonstrating that a concentration gradient takes place in the pool and should thus be investigated.

To confirm this gradient, we measured concentrations at several depths after the test. The concentration near the pool's surface was always lower than the ones measured near the bottom of the pool.

### 3.4. Influence of other Parameters

The above paragraph focused on the reference test for small scale tests, but it is important to evaluate whether the proposed model (§ 5) enables the taking into consideration the influence of the different parameters. The other small-scale tests were then compared with the new approach for evaporation rate evaluation.

Two main parameters' influences were tested during the small-scale tests. The first parameter tested was the initial pool concentration. Reducing the initial concentration, test no. 1 was expected to reduce the initial evaporation rate and consequently the kinetics of the gradient formation in the liquid phase. This was confirmed by experimental measurements at lower concentrations in tests no.

1 and 2 (compare Figure 8 below with Figure 6). The experimental curve on this figure indicates a smoother variation of the evaporation rate in the first 20 min. This curve also shows that the proposed model is in line with the experiment, even though it over-estimated the evaporation rate in the first 5 min.

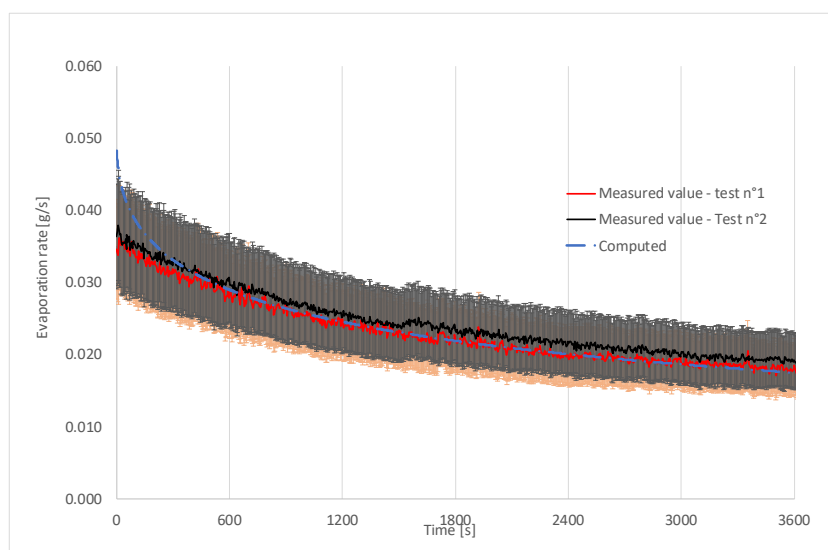


**Figure 8.** Evolution of the evaporation rate for test no. 1 and test no. 2 (repeatability).

Finally, it is important to verify the repeatability of the experiments. This was done by comparing data from tests no. 1 and 2. Figure 8 shows that they had the same evaporation rate and evolution tendency. The gray and orange zones correspond to the interval of uncertainty.

The second parameter that was tested was the ambient velocity. Figure 9 below shows the evaporation rate measurement for test no. 4 that corresponded to a 1.5 m/s ambient velocity compared to the reference test. As for previous figures, the uncertainty interval is plotted in orange and grey. This confirms that increasing the ambient velocity leads to an increase in the evaporation rate. This test also shows that the equilibrium reached after 20 min was quite independent of the velocity. On the other hand, test no. 5 led to a reduction of the evaporation rate, about 0.02 g/s after 2400 s. It was not plotted on this curve; we preferred to give an uncertainty domain for each test. The curve also shows that the model tends to overestimate the evaporation rate.

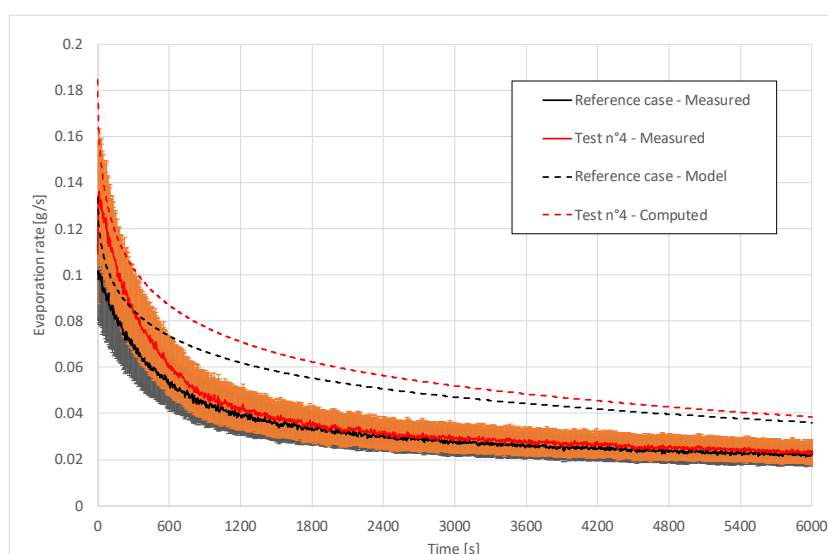


**Figure 9.** Evaporation rate over time: small-scale evaluation of the velocity influence. Test no. 4 corresponds to 1.5 m/s ambient air velocity.

These curves confirm that the proposed model enables the prediction of the evaporation rate evolution over time with accuracy, as well as reproduction of the influence of the different parameters that govern the evaporation rate. In most cases, the model over-predicted the real evaporation rate, which is a prudent approach when dealing with risk management and land use planning.

#### 4. Medium-Scale Experiment Results

##### 4.1. Scale Factor Influence

The previous chapter highlighted that predicting the evaporation rate of an ammonia pool requires considering the concentration gradient in the pool together with the temperature evolution. This result was based on small-scale consideration, and the influence of the scale factor should be assessed. Considering the reference test cases, the first quantity to compare is the evaporation rate per unit area (ERPUA) for both scales, obtained by dividing the measured evaporation rate by the pool surface. The comparison of ERPUA is presented in Figure 10. Orange and grey curves represent the uncertainty interval.

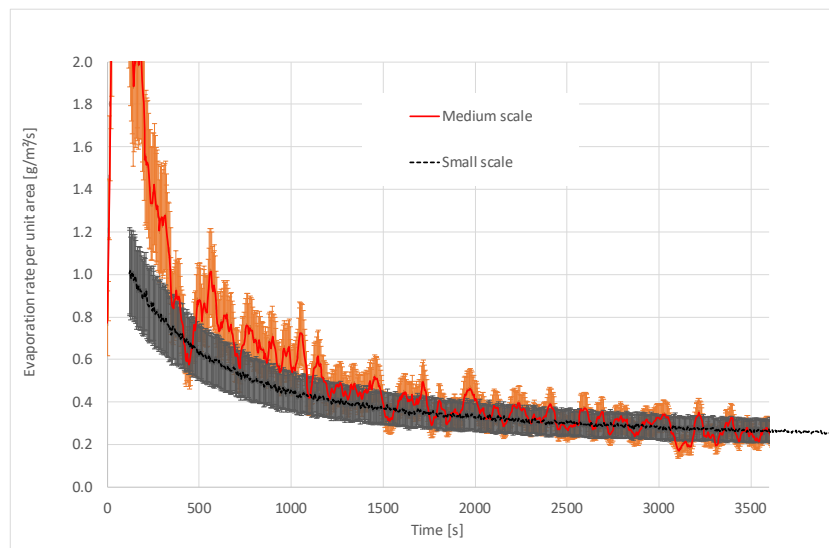


**Figure 10.** Evaporation rate per unit area: reference configuration for small and medium scales.

This first comparison showed that the dependence of evaporation rate to pool area was low; this confirms the Froude scaling approach. This is of primary importance in order to use the conclusion of this study for large-scale configurations. It should be noted that the difference observed during the first 250 s was induced by the filling of the pool; the flow of liquid lasted longer in time and produced more disturbances for medium-scale tests.

It is also important to evaluate the influence of the scale factor on the temperature gradient along the pool's depth. As mentioned previously, this gradient was negligible for small case situations; this was also confirmed for medium-scale tests, as shown in Figure 11.

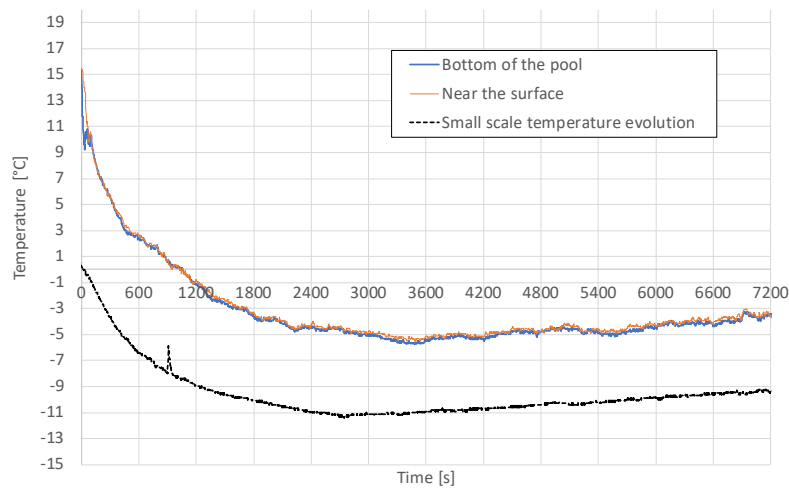


**Figure 11.** Temperature evolution along time for the three measured depths.

The temperature evolution measured during the small-scale tests and the medium-scale tests show the similarity in terms of dynamics. Values were different since initial temperatures differed.

#### 4.2. Influence of the Pool Exposed Length

The last parameter tested was the pool dimension in order to evaluate whether the exposed wind pool length (hereafter referred to as “exposed length”) influenced the evaporation rate. In the experimental configuration of test no. 3, the surface was fixed to 2 m<sup>2</sup> by keeping the width equal to the reference test and increasing only the exposed length. The relevant quantity to be compared in such a situation is the ERP UA. Should the exposed length influence the ERP UA, this quantity should decrease when increasing the length because the concentration of ammonia above the pool would increase with distance [22]. Such a trend was not detected experimentally (see Figure 12). This comparison highlights the fact that the exposed pool length did not strongly influence the evaporation rate.

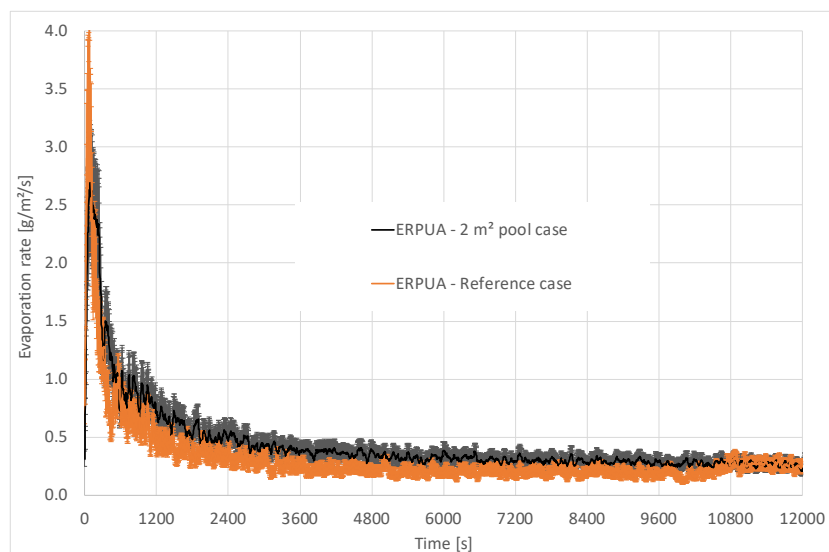


**Figure 12.** Evolution of the evaporation rate as a function of the exposed pool length.

#### 4.3. Influence of the Surrounding Turbulence

The first parameter studied was the surrounding turbulence. Since the mass evaporation process is governed by the modification of the concentration just above the pool, the influence of the

turbulence intensity on the evaporation rate was measured by conducting test no. 4. The evaporation rate for this configuration, compared to the reference one, is shown in Figure 13. Again, the uncertainty interval is plotted in orange and grey on the curve.

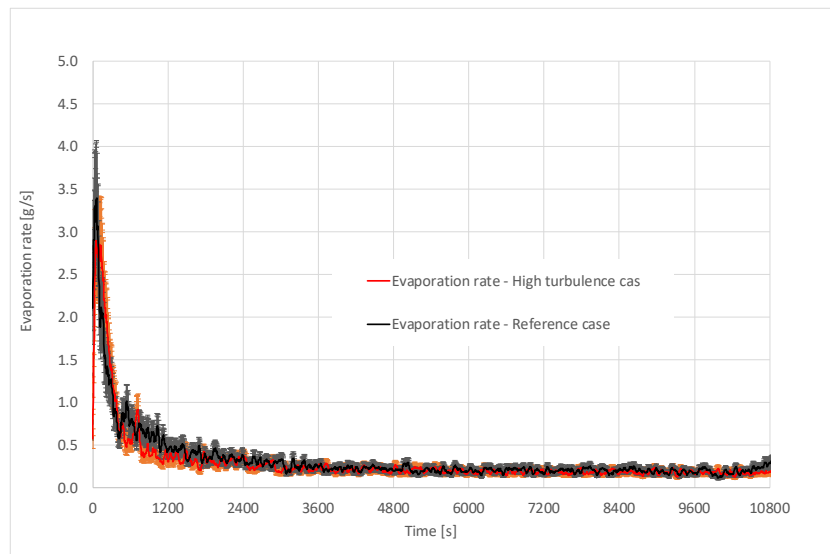


**Figure 13.** Influence of local upstream turbulence on the evaporation rate.

This comparison shows that increasing the turbulence intensity just above the pool is not of primary importance when dealing with the evaporation rate. These turbulent fields are of course quite artificial.

*4.4. Influence of the Wind Velocity*

Test no. 2 was conducted to assess the effect of increasing wind velocity from 1.0 m/s to 1.5 m/s. The evolution of the evaporation rate for this velocity value is plotted in Figure 14, together with the reference case. The predicted evaporation rate, using the proposed model (see Section 5), is also plotted on this figure.

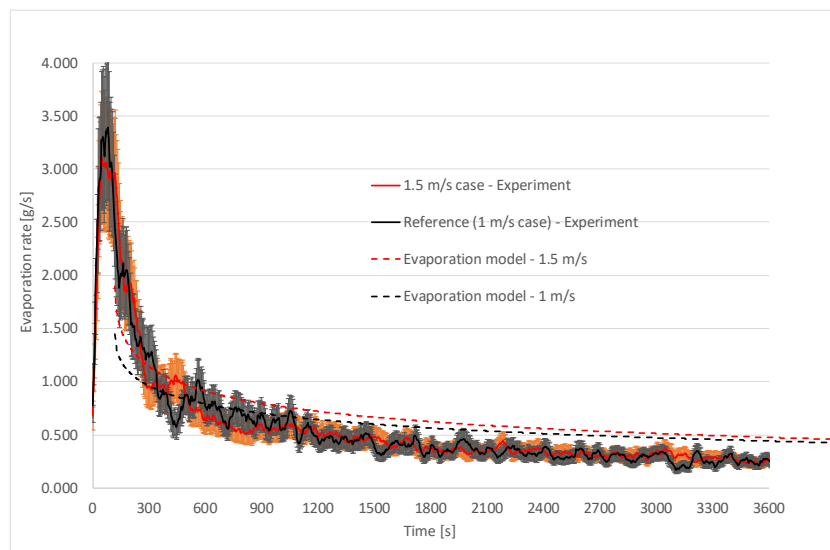


**Figure 14.** Evolution of evaporation rate for two velocity configurations.

This case confirms the conclusion of the small-scale experiment and also confirms the relevance of the physical approach proposed with a model able to predict the evaporation rate’s evolution over time.

## 5. Proposition of an Evaporation Model

### 5.1. Physical Aspect

The experimental study presented in this paper suggests that evolution of evaporation rate over time should be estimated considering pool concentration evolution and associated gradient along the pool's depth. Thus, going back to the physical process is useful. Dealing with the mass concentration of a species in a solution, here ammonia, we can write the conservation equation as

$$\frac{\partial \rho \cdot Y_k}{\partial t} + \frac{\partial \rho \cdot U_i \cdot Y_k}{\partial x_i} = \frac{\partial}{\partial x_i} \rho D_k \frac{\partial Y_k}{\partial x_i} + \rho \omega_k \tag{3}$$

In this equation,  $\rho$  is the fluid density;  $Y_k$  is the  $k$ -species mass fraction;  $U_i$  is the velocity component in  $x_i$ -direction;  $D_k$  is the diffusion coefficient of  $k$ -species; and  $\omega_k$  is the production or consumption term for  $k$ -species, for the present case, the evaporation rate on the interface. This equation clearly highlights the mechanisms that take place in the pool—the evaporation is governed by the diffusion process. The sinking of ammonia in the liquid pool occurs near the pool's surface; the concentration gradient forms with concentration near the surface lower than the one near the bottom. Such a gradient might strongly influence the evaporation rate according to the strong evolution of the vapor pressure as a function of ammonia concentration.

### 5.2. Development of a Predictive Tool: EVAP-Tox

To take this phenomenon into account, we require a specific numerical tool. This tool should allow us to solve the evaporation rate coupled with the pool behavior in terms of concentration and temperature. The skeleton of this model (EVAP-Tox) is represented in Figure 15.

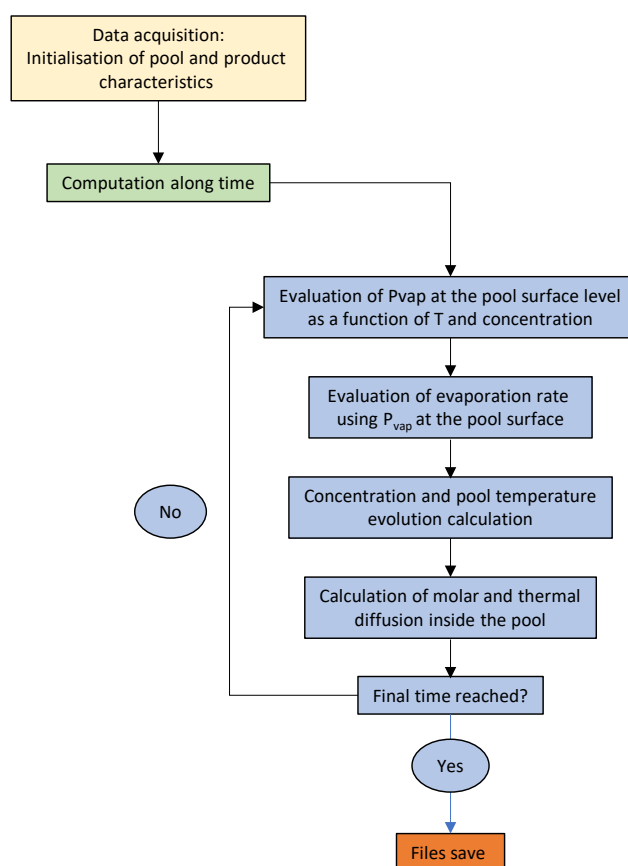


Figure 15. Skeleton of evaporation model.

Input data for the model are the pool dimensions, its depth, the ammonia pool concentration, the pool, and ambient temperature, assuming both the pool temperature and ambient temperature are identical, the air velocity, and the required simulated time. The four computation steps are detailed below.

First, the vapor pressure is estimated considering both pool surface temperature and concentration following the curve proposed by [23].

Then, the evaporation rate,  $\omega_k$  in the equation, is estimated using the Mackay and Matsugu correlation. In this relation, the vapor pressure is the one computed with the pool surface characteristics. This also enables the estimation of the sink term of ammonia and energy for the pool surface.

The concentration and temperature gradients inside the pool are then estimated, following a 1D finite difference discretization. The equation is solved using a first-order scheme in time with a full explicit approach, and a second-order finite difference scheme for the diffusion term in space. The species concentration equation (Equation (3)) is simplified to a diffusion relation, assuming that convection is negligible with the assumption of constant density:

$$\frac{\partial Y_k}{\partial t} = D_k \frac{\partial^2 Y_k}{\partial x_i^2} + \omega_k \quad (4)$$

It must be added that the liquid density rises when the ammonia concentration diminishes with a convective movement in the pool. A constant was then added to increase the diffusion velocity while keeping a 1D approach. The constant was found to be 50 using the small-scale reference test; its value was then kept constant for comparison with other cases.

The temperature,  $T$ , is also solved using a diffusion equation:

$$\frac{\partial T}{\partial t} = \frac{\lambda}{\rho \cdot C_p} \frac{\partial^2 T}{\partial x_i^2} + \omega_{tk} \quad (5)$$

In this equation,  $\lambda$  is the thermal conductivity,  $C_p$  is the specific heat of ammonia, and  $\omega_{tk}$  is the sink term of energy, since for this equation the cooling is due to the phase change process. As for species, this equation is solved using an explicit approach—first order in time and second order in space using a finite difference scheme.

### 5.3. Some Results of the Model

Using EVAP-Tox, the concentration can be calculated in the pool as a function of the pool's depth. An example of the concentration gradient calculated after 1 hour for the reference small scale case is given below (Figure 16), where 0 is the free surface of the pool. The evolution of concentration rate along the depth of the pool was computed over each "time step".

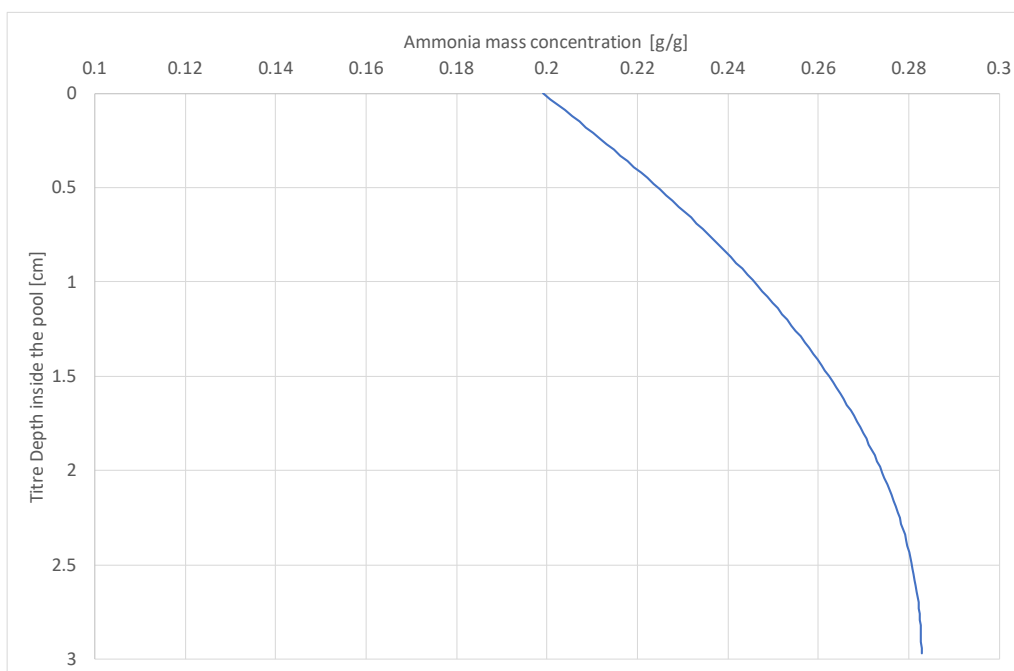


**Figure 16.** Ammonia concentration along the pool depth; 0 is the pool surface.

This enables evaluating the mass flow rate of ammonia over time using the computed quantities near the surface. A comparison of the computed value of the evaporation rate with the measured rate is presented in Figure 17.

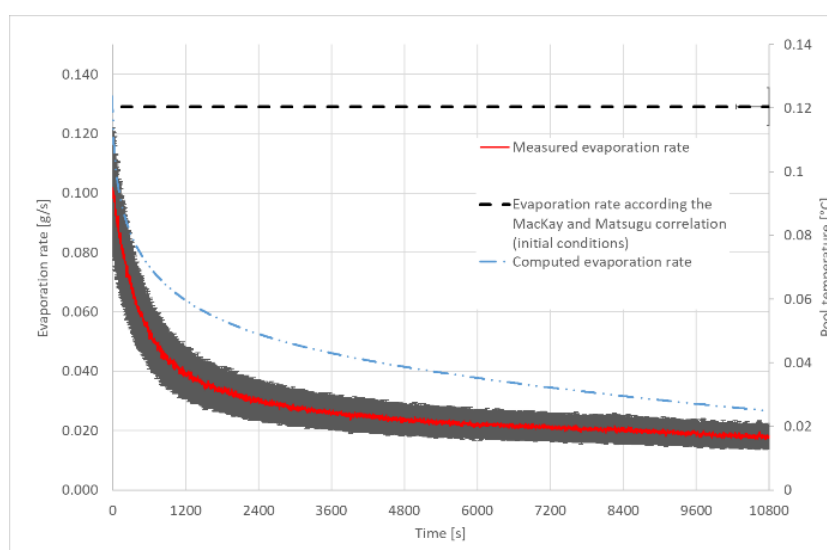


**Figure 17.** Time evolution of evaporation rate measured during the reference small-scale tests and calculated with the proposed model.

This comparison shows that taking into account the influence of the diffusion equilibrium in the liquid pool allowed us to predict the evaporation rate over time. The approach, based on the correlation presented by MacKay and Matsugu [3] at each time step while taking into account the temperature and surface concentration evolution, enables us to predict a conservative evaporation rate since the computed value is always higher than the measured rate.

## 6. Conclusions

As mentioned in the introduction, the main objective of this experimental study was to establish the evolution of ammonia solution evaporation rate over time. This objective was definitely met since

all the tests conducted highlighted a strong reduction of the evaporation rate in the first 60 min after establishing the pool; this reduction was around 80%. On the basis of the available measures and considering the physical phenomena that takes place in the pool, we proposed a physical explanation of this reduction. Considering the evaporation mechanism that occurs close to the pool's surface, and the diffusion phenomena in the vertical direction into the pool, we can assume that a concentration gradient appeared in the pool after evaporation starts. This gradient was confirmed using three samplings at three different heights in the pool. In parallel, it was confirmed that no vertical temperature gradient should be considered.

Using the same experimental setup, the influence of some well-known parameters was confirmed. Typically, increasing the solution concentration or atmospheric velocity leads to an increase in the evaporation rate. The tests, however, highlight that, independent of the ambient conditions, the evaporation rate strongly decreased within the first minutes. During this series of tests, local turbulence was shown to have no significant effect on the evaporation rate.

These experiments demonstrated that the rate of evaporation of liquid pools containing ammonia does not depend on the pool area while respecting the Froude scaling. This observation is crucial as it confirms the possibility of applying the proposed model to larger scale evaporating pools. This independence confirms that the Froude scaling used during this study is relevant.

This experimental work shows clearly that the numerical approach considering a constant evaporation rate for ammonia gives overly conservative results.

The proposed model, EVAP-Tox, which consists of evaluating the evaporation rate as a function of time on the basis of the Mackay and Matsugu correlation, is relevant since the concentration and temperature evolution in the pool were considered.

For more accurate results, the evolution of pool concentration should also be estimated not only over time but also as a function of pool depth, since a significant concentration gradient appears in this direction. As a reminder, the evaporation correlation is based on an average velocity of external flow as the influencing parameter regarding flow dynamics. A further improvement may consist in adding a new module that would evaluate the diffusion process in the surrounding air more accurately.

**Author Contributions:** The different authors had a different role in this research topic. Véronique DEBUY and Jean-Pierre BERTRAND were in charge of investigation with the experimental tests; Benjamin TRUCHOT built the model and wrote the original draft; André CARRAU and Thibault PENELON were in charge of writing and reviewing the paper. They were also involved in the scientific development. All authors have read and agreed to the published version of the manuscript.

**Funding:** This research received no external funding

**Conflicts of Interest:** The authors declare no conflict of interest

## References

1. Sutton, O.G. Wind structure and evaporation in a turbulent atmosphere. *Proc. R. Soc. London. A* **1934**, *146*, 701–722, doi:10.1098/rspa.1934.0183.
2. Kunsch, J. Two-layer integral model for calculating the evaporation rate from a liquid surface. *J. Hazard. Mater.* **1998**, *59*, 167–187, doi:10.1016/s0304-3894(97)00145-3.
3. Mackay, D.; Matsugu, R.S. Evaporation rates of liquid hydrocarbon spills on land and water. *Can. J. Chem. Eng.* **1973**, *51*, 434–439, doi:10.1002/cjce.5450510407.
4. Blanchard, A.; Hadlock, D. *Source Term Determination for Spills of Binary Liquid Solutions*; Technical Report WSRC-TR-96-0404; Westinghouse Savannah River Company: Aiken, SC, USA, 1997.
5. Opschoor, G. *Evaporation, Methods for the Calculation of Physical Effects*, 1st ed.; Yellow book, Chapter 5, TNO, GEVAARLIJKE STOFFEN: Amsterdam, Netherland, 1978.
6. Brighton, P.W.M. Evaporation from a plane liquid surface into a turbulent boundary layer. *J. Fluid Mech.* **1985**, *159*, 323, doi:10.1017/s0022112085003238.
7. Woodward, J.L. An integrated model for discharge rate, pool spread, and dispersion from punctured process vessels. *J. Loss Prev. Process. Ind.* **1990**, *3*, 33–37, doi:10.1016/0950-4230(90)85020-a.

8. Van den Bosch, C.J.M.; Weterings, R.A.P.M. *“Yellow Book”, Methods for the Calculation of Physical Effects Due to Releases of Hazardous Materials (Liquids and Gases)*, 3rd ed.; Committee for the Prevention of Disasters, TNO, GEVAARLIJKE STOFFEN: Amsterdam, Netherland, 1997.
9. Brambilla, S.; Manca, D. Accidents involving liquids: A step ahead in modeling pool spreading, evaporation and burning. *J. Hazard. Mater.* **2009**, *161*, 1265–1280, doi:10.1016/j.jhazmat.2008.04.109.
10. Bubbiso, R.; Mazzarotta, B. Predicting Evaporation Rates from Pools. *Chem. Eng. Trans.* **2016**, *48*, doi:10.3303/CET1648009.
11. Mackay, D.; van Wesenbeeck, I. Correlation of chemical evaporation rate with vapor pressure. *Environ. Sci. Technol.* **2014**, *48*, 10259–10263.
12. Salin, A.A.; Galeev, A.D.; Ponikarov, S.I. Study of the Evaporation of Hydrochloric Acid: Modeling and Experiment. *J. Eng. Phys. Thermophys.* **2014**, *87*, 753–762, doi:10.1007/s10891-014-1069-2.
13. Fingas, F. Studies on the evaporation of crude oil and petroleum products: I. the relationship between evaporation rate and time. *J. Hazard. Mater.* **1997**, *56*, 227–236.
14. Okamoto, K.; Watanabe, N.; Hagimoto, Y.; Miwa, K.; Ohtani, H. Changes in evaporation rate and vapor pressure of gasoline with progress of evaporation. *Fire Saf. J.* **2009**, *44*, 756–763, doi:10.1016/j.firesaf.2009.03.004.
15. Forestier, S. Etude de L'évaporation d'un Liquide Répandu au Sol Suite à la Rupture D'un Stockage Industriel. Ph.D. Thesis, Ecole Nationale Supérieure des Mines de Saint-Etienne, Saint-Étienne, France, 2012. (In French).
16. Mózer, V.; Holla, K.; Buganová, K. Determination of Ammonia Evaporation Rates for MOPORI Project Model. *Adv. Mater. Res.* **2014**, *1001*, 458–462, doi:10.4028/www.scientific.net/amr.1001.458.
17. Mikesell, J.L.; Buckland, A.C.; Diaz, V.; Kives, J.J. Evaporation of contained spills of multicomponent nonideal solutions. In Proceedings of the International Conference and Workshop on Modeling and Mitigating the Consequences of Accidental Releases of Hazardous Materials, New Orleans, LA, USA, 20–24 May 1991.
18. Corruchaga, A.; Casal, J. Evaporation of ammonia from aqueous solution spills. In Proceedings of the 14th International Conference on Environmental Science and Technology, Rhodes, Greece, 3–5 September, Global Network for Environmental Science and Technology, Lekkas, 2015.
19. Truchot, B. *Fire Safety Sciences News 38*; International Association for Fire Safety Science: Walse, England, 2015.
20. Mac Caffrey, B.J. *Purely Buoyant Diffusion Flames: Some Experimental Results*; NBSIR 79-1910 Report; National Institute of Standards and Technology: Gaithersburg, MD, USA 1979.
21. Tamanini, F. Turbulence effects on dust explosion venting. *Plant/Operations Prog.* **1990**, *9*, 52–60, doi:10.1002/prsb.720090111.
22. Pénelon, T.; Debuy, V.; Truchot, B.; Wagner, C.; Donnat, L.; Lechaudel, J.-F. Pool evaporation: Experimental tests at medium-scale with gasoline. *J. Loss Prev. Process. Ind.* **2020**, *65*, 104072, doi:10.1016/j.jlp.2020.104072.
23. Senior, J.; Guest, R.A.; Wood, W.E. *Kirk-Othmer Encyclopedia of Chemical Technology*; John Wiley & Sons, Inc.: Hoboken, NJ, USA, 2000.

**Publisher's Note:** MDPI stays neutral with regard to jurisdictional claims in published maps and institutional affiliations.



© 2020 by the authors. Licensee MDPI, Basel, Switzerland. This article is an open access article distributed under the terms and conditions of the Creative Commons Attribution (CC BY) license (<http://creativecommons.org/licenses/by/4.0/>).